Conformations and Order in Atactic Poly(vinyl chloride) Melts from Molecular Dynamics Simulations

Grant D. Smith

Eloret Institute, Sunnyvale, California 94087

Richard L. Jaffe

NASA Ames Research Center, Moffett Field, California 94035

Do Y. Yoon*

IBM Almaden Research Center, 650 Harry Road, San Jose, California 95120-6099

Received June 29, 1992; Revised Manuscript Received October 16, 1992

ABSTRACT: Molecular dynamics simulations of atactic poly(vinyl chloride) (PVC) melts at 450 and 600 K were performed including individual hydrogens and utilizing an ab initio quantum chemistry based force field. Electrostatic interactions were considered by employing partial atomic charges with a distance-dependent dielectric constant. The effects of polar electrostatic interactions and packing on chain conformations and intermolecular orientational correlations were examined individually by performing additional simulations of isolated chains and melts without intermolecular Coulombic interactions. Pair distribution functions show strong temperature dependence but are relatively insensitive to electrostatic interactions. Reasonably good agreement between calculated and experimental X-ray scattering profiles is found for PVC melts at 450 K. Chain conformations in PVC melts are found to be extended relative to the conformations of isolated chains. Moreover, significant temperature-dependent orientational order is seen in PVC melts, with highly parallel chain segments being distributed in small localized clusters. These deviations from the unperturbed chain model are attributable to the presence of polar intermolecular interactions in PVC melts.

Introduction

Atomistic molecular dynamics (MD) simulation techniques have been used extensively in recent years to study equilibrium and dynamic properties of polymer melts and glasses. Recent applications include investigations of the glass transition,[1] short-range order and orientation correlation,[2] polymer glasses at interfaces,[3] local chain dynamics,[4-6] P-V-T behavior,[7] small-molecule diffusion,[8] and flexible side-group motion.[9] So far, these MD simulations of synthetic polymers have been limited primarily to polyolefins, which are both simple chemically and nonpolar. In simulations of polyolefins, methyl and methylene groups are often represented by spherically symmetric "united" atoms, thereby greatly reducing the number of degrees of freedom and eliminating high-frequency vibrational modes involving hydrogen atoms. In addition, representation of electrostatic interactions need not be considered in nonpolar polyolefin systems. Many technologically important polymers, however, exhibit strong polar interactions. Thus, an important step toward MD simulations of these polymers is the inclusion of these polar interactions in simulations in a computationally viable manner. Accurate treatment of polar interactions precludes the use of united-atom potentials when considering partial charges and hence requires greater computational resources.

The primary purpose of this work is to examine chain conformations and intermolecular orientational order in atactic poly(vinyl chloride) (PVC) melts by MD simulation as a first example of polar polymer systems. Many unanswered questions remain regarding molecular order and structure in atactic PVC, which are exhibited most clearly in the thermoreversible gelation behavior[10] and "crystallinity" observed by thermal analysis[11] in atactic PVC glasses. An earlier molecular mechanics simulation study indicated the existence of a certain degree of parallel-chain alignment in atactic PVC glass.[12] However, the molecular mechanics approach was unsuccessful in reproducing the experimental X-ray scattering profiles and chain conformations. A recent molecular mechanics study of PVC glasses,[13] which utilized MD at a very high temperature as part of the equilibration procedure, was also unsuccessful in reproducing chain conformations. Our approach involves MD simulation techniques utilizing a recently parametrized force field based upon ab initio quantum chemistry calculations. Future work will include extension to larger systems of higher molecular weight and investigations of MD generated PVC glasses.

Simulation Methodology

Force Field. In other papers[14,15] we discuss in detail derivation of an atomic force field applicable to PVC. Intramolecular force-field parameters, namely, stretch, bend, torsion, and intramolecular nonbonded (including partial atomic charges) terms, were obtained from ab initio quantum chemistry calculations on model molecules and their complexes. The following procedure was employed: first, the stretch and bend parameters were determined from calculations of the harmonic force constants for the two lowest energy 2,4-dichloropentane conformers; second, the nonbonded parameters were determined by least-squares fits to the dipole moments of 2-chloropropane (CP), 1,3-dichloropropane (DCP), and CP/CP and CP/DCP complex energies; last, the torsional parameters were adjusted to reproduce the relative 2,4-dichloropentane conformer energies and rotational barrier heights. It was found that the ab initio calculations tended to somewhat underestimate the attractive nonbonded dispersion interactions.[14,15] While this shortcoming has only a minor effect in determining intramolecular conformations, it has a large effect on bulk properties such as cohesive energy and pressure, which depend strongly on the magnitude of the intermolecular nonbonded interactions. Therefore,

0024-9297/93/2226-0298$04.00/0

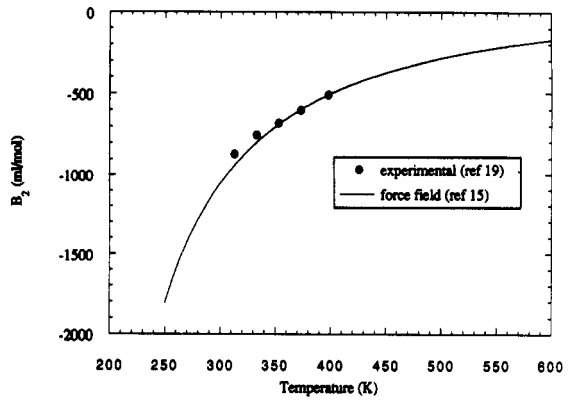

Figure 1. Second virial coefficient values for 2-chloropropane. The filled circles indicate experimental values; the solid line indicates calculated values utilizing the partial charges and intermolecular LJ parameters summarized in Table II.

Table I
Force-Field Parameters for Bonded Interactions

stretch[a]	k_s (kcal/mol/Å^2)	r_{ij}^0 (Å)
C–C	618	1.53
C–H	704	1.09
C–Cl	376	1.83
bend[b]	**k_b (kcal/mol/rad^2)**	**θ_{ijk}^0 (rad)**
C–C–C methylene centered	170	112.0
C–C–C methine centered	170	108.2
C–C–H	104	106.3
H–C–H	108	109.0
C–C–Cl	126	106.3
Cl–C–H	128	103.0
torsion[c]	**B_1 (kcal/mol)**	**B_3 (kcal/mol)**
C–C–C–C racemic	0.5	1.4
C–C–C–C meso	0.2	2.2

[a] $U(\text{stretch}) = (1/2)k_s(r_{ij} - r_{ij}^0)^2$. [b] $U(\text{bend}) = (1/2)k_b(\theta_{ijk} - \theta_{ijk}^0)^2$. [c] $U(\text{torsion}) = (1/2)B_1(1 - \cos\phi) + (1/2)B_3(1 - \cos 3\phi)$.

Table II
Force-Field Parameters for Nonbonded Interactions

electrostatics	partial charge (esu)	electrostatics	partial charge (esu)
methyl group	0.0094	chlorine	−0.1987
methylene carbon	−0.1792	methylene hydrogen	0.0990
methine carbon	0.0313	methine hydrogen	0.1486

nonbonded dispersion[a]	intramolecular		intermolecular	
	r_{ij}^0 (Å)	ξ_{ij} (kcal/mol)	r_{ij}^0 (Å)	ξ_{ij} (kcal/mol)
methyl group	4.1752	0.1419	4.0486	0.2910
carbon	3.9197	0.0540	3.8001	0.1107
chlorine	3.9720	0.1608	3.8513	0.3298
hydrogen	3.2126	0.0086	3.1150	0.0177

[a] Parameters for crossterms are obtained by taking the arithmetic average of the r_{ij}^0 values and the geometric mean of the ξ_{ij} values.

in order to improve the quality of the intermolecular nonbonded parameters, we modified slightly the force field due to Williams[16-18] in order to optimize agreement between calculated and experimental second virial coefficient data for 2-chloropropane,[15] as shown in Figure 1. Force-field parameters are summarized in Tables I and II.

Nonbonded Interactions. Nonbonded dispersion interactions are represented as a sum of two-body Lennard-Jones (LJ) terms of the form

$$E^{LJ}(r_{ij}) = \xi_{ij}[(r_{ij}^0/r_{ij})^{12} - 2(r_{ij}^0/r_{ij})^6] \qquad (1)$$

where r_{ij} is the separation between atoms i and j. Intramolecular nonbonded interactions are considered only when atoms i and j are separated by two or more intervening atoms. For polar Coulombic interactions, dielectric screening effects are accounted for by introduction of a distance-dependent dielectric constant, based the Block–Walker model,[20] that has been used in previous molecular mechanics simulations.[12,21] In this model, the effective dielectric constant is taken to be unity up to some critical charge separation distance beyond which screening effects become important. The dielectric constant then approaches a bulk value ϵ_b exponentially as given by the relationship

$$\epsilon(r_{ij}) = \epsilon_b \exp(-a_{ij}/r_{ij} \ln \epsilon_b) \qquad r_{ij} > a_{ij} \qquad (2)$$

where a_{ij} is the critical separation distance. The Coulombic energy is then given by[12,21]

$$E^C{}_{ij}(r_{ij}) = \frac{q_i q_j}{\epsilon(r_{ij}) r_{ij}} \qquad (3)$$

Following previous investigators,[12,21] the critical distance a_{ij} was assumed to be correlated with the van der Waals diameters of the interacting species. As in a previous simulation,[21] a single value for the critical charge separation was used independent of the particular interacting species (specifically 3.85 Å, corresponding to the chlorine van der Waals diameter). For the bulk dielectric constant we used $\epsilon_b = 3.5$, corresponding to the dielectric constant of PVC glass. Chain conformations and intermolecular orientational order were found to be relatively insensitive to the precise value of ϵ_b.

Nonbonded Truncation. In order to limit the number of interatomic interactions without seriously affecting thermodynamic and structural properties, we have employed a spherical nonbonded truncation with a switching function. In MD simulations of liquid water[22] it has been found that a truncation radius $r_t = 6$ Å is sufficient to eliminate truncation distance dependencies in the thermodynamic properties and molecular order. MD studies of simple dipolar fluids also indicate that the spherical truncation method using a cutoff of 2.6σ is adequate,[23] where σ is the van der Waals diameter. In these cases, the range of significant influence of these interactions is greater than that of the dispersion interactions, which is often considered to be limited to the van der Waals diameter of the atoms (usually less than 4 Å). We have found that $r_t = 9$ Å is adequate for PVC, with computed properties being influenced only slightly by increasing r_t to 11 Å. Investigation of a significantly larger truncation radius was not feasible due to current computational constraints.

While it is a common practice to scale the Coulombic energy smoothly to zero at r_t via application of a switching polynomial,[12,22] we have chosen an alternative approach. We scale the Coulombic force smoothly to zero, which is equivalent to scaling the energy to a constant value, given by the energy (eq 3) at r_t, $E^C{}_{ij}(r_t)$. When the Coulombic energy is scaled to zero over some relatively short distance near r_t (usually on the order of 1 Å), unphysically large forces can result in the scaling region. This can result in artificially induced features in the pair distribution functions for separations near the truncation distance as the partially charged atoms react to these spurious forces. This effect can be eliminated by either application of the truncation based upon charge neutral residues or by smoothly scaling the energy to $E^C{}_{ij}(r_t)$ at the truncation distance, where $E^C{}_{ij}(r_t)$ is dependent upon the nature of interaction atoms. The first option works well for small molecules such as water but leads to difficulties in extended-chain molecules in that charge neutral residues are not uniquely defined.

In order both to scale the energy smoothly to $E^C{}_{ij}(r_t)$ at r_t and to smoothly cross over from a dielectric constant of unity to a distance-dependent Block–Walker value, the

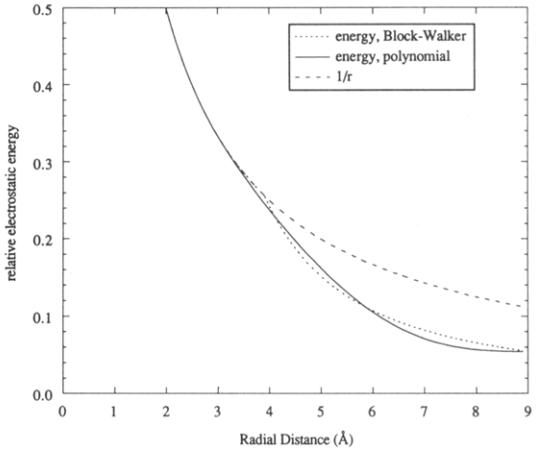

Figure 2. Block–Walker and polynomial representation of Coulombic energy, compared with the energy from eq 3 with $\epsilon(r_{ij}) = 1$. In all cases $q_i = q_j = 1$.

"scaled" Coulombic energy was represented in the following fashion:

$$E^{S}_{ij}(r_{ij}) = \frac{q_i q_i}{r_{ij}} - E^{C}_{ij}(r_t) \qquad r_{ij} < r_s \tag{4}$$

$$E^{S}_{ij}(r_{ij}) = \frac{q_i q_i}{r_{ij}} S(r_{ij}) + [1 - S(r_{ij})]E^{C}_{ij}(r_t) - E^{C}_{ij}(r_t) \qquad r_s \le r_{ij} \le r_t \tag{5}$$

$$E^{S}_{ij}(r_{ij}) = 0 \qquad r_{ij} > r_t \tag{6}$$

where r_s is a parameter and $S(r_{ij})$ is a quintic switching polynomial with the properties $S(r_s) = 1$, $S(r_t) = 0$, $S'(r_s) = 0$, $S'(r_t) = 0$, $S''(r_s) = 0$, and $S''(r_t) = 0$. The constant term $E^{C}_{ij}(r_t)$ is subtracted from the energy in order to eliminate energy fluctuations which would otherwise occur when particle separations cross the truncation radius. This does not affect the Coulombic forces or the consequent MD trajectories. The parameter r_s is adjusted so as to yield the best agreement between eqs 4–6 and eq 3. Figure 2 is a comparison of the Coulombic energy from eqs 4–6 and 3 (before subtraction of $E^{C}_{ij}(r_t)$) for a value $r_s = 3$ Å. Also shown is the energy resulting from a dielectric constant of unity. The Coulombic force is readily obtained from the gradient of the energy.

Ensemble. In the present study, MD simulations were preformed on an ensemble of 30 atactic PVC molecules of 12 repeat units each with terminal methyl groups generated using a Monte Carlo technique[24] by assuming Bernoullian statistics. The average meso diad fraction of the chains was 0.45, which corresponds to a polymerization temperature of 50 °C.[25] In the MD simulations all atoms were considered explicitly except for the terminal methyl groups which were treated as united atoms, resulting in a total of 2130 force centers.

Molecular Dynamics. The initial configuration of the system was obtained by placing the PVC chains in an extended conformation in a low-density periodic system. The system was then disordered at high temperature (750 K) via MD. Canonical averages at constant density were obtained at 600 and 450 K by utilizing the constant-temperature algorithm of Nosé.[26] Integration was via a third-order method described in detail in the appendix. Periodic boundary conditions were employed, with a box dimension of 31.27 Å at 450 K. The system density was 1.24 and 1.11 g/cm^3, at 450 and 600 K, respectively. These values represent best estimates of densities for high molecular weight PVC. The value at 450 K was obtained

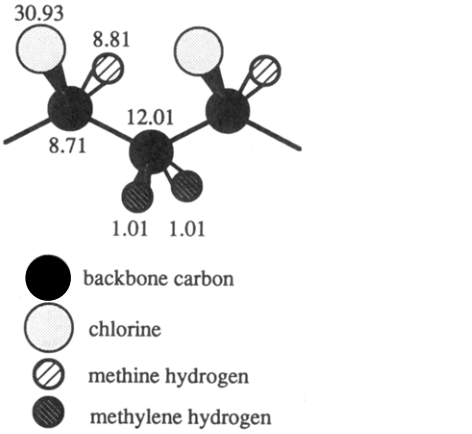

Figure 3. Atomic masses for a PVC repeat unit as assigned for MD simulations.

from extrapolation of experimental data which is available up to 420 K.[27] The density at 600 K was determined by assuming a bulk thermal expansion coefficient of 8×10^{-4}/K for temperatures above 450 K, a typical value for polyolefin melts.

In order to utilize a reasonably long time step (3 fs), high-frequency vibrations were constrained as follows. The standard SHAKE algorithm[28] was used to constrain backbone, chlorine and methine hydrogen bond lengths. Methylene hydrogens were completely constrained using the method of Ryckaert et al.,[29] where, in addition to constraining the C–H bond lengths, the methylene hydrogens are constrained to lie in a plane perpendicular to the C–C–C plane (plane of the figure in Figure 3), with the C–H bonds constrained to a constant angle with respect to the bisector of the C–C–C bond angle. The frequencies of the bending modes involving the chlorines and methine hydrogens were reduced by redistributing the mass of the methine group among the constitutive particles. This was done in such a manner as to leave the total mass of the methine group and moment of inertia for rotation about the skeletal bonds involving the methine group unchanged. The resulting atomic masses are indicated in Figure 3. The frequencies of the bending modes involving the methine group are subsequently reduced without requiring reduction of the bending force constants or constraint of the corresponding motions, with a smaller effect on equilibrium properties than either of these common methods of eliminating high-frequency motions. This is more important for the sterically large chlorine atom than for the relatively small hydrogens in that the chlorine has a greater influence on torsional rotational barriers and conformational energies.

The equilibration time at each temperature was approximately 1 ns. A sampling run was 100 ps. Conformational properties represent averages over a series of 5 or 6 sampling runs, while pair distribution functions and orientational correlations are computed from single runs, as these properties do not change significantly after equilibration. Simulations were performed on an IBM RISC 6000 Model 540. Simulation pressures were on the order of 500 atm, which is reasonable considering that experimental densities of a high molecular weight system were imposed on a low molecular weight system. The cohesive energy density at 450 K of approximately 8×10^4 kcal/m^3 lies 10–30% below experimental values for room-temperature PVC glasses.[30] These results indicate that the force field does a credible job in reproducing P–V–T behavior of PVC melts. We reserve detailed discussion of the P–V–T behavior of PVC melts and glasses for a future paper where a higher molecular weight system will be considered.

Table III
Chain Conformations

temp (K)	melt	melt w/o Coulomb[a]	isolated	RIS[b]
		Characteristic Ratio		
450	8.2 ± 0.5	7.6 ± 0.6	7.4 ± 0.4	7.4
600	7.4 ± 0.6	7.3 ± 0.5	6.8 ± 0.4	6.4
		Fraction of Trans Bonds		
450	0.710	0.702	0.682	0.704
600	0.682	0.673	0.655	0.656

[a] Melt simulations performed excluding intermolecular Coulombic interactions. [b] From the rotational isomeric state model of Mark.[32]

In addition to simulations of the system with the full intermolecular potential, melt simulations without intermolecular Coulombic forces (but retaining dispersion forces) were also performed via MD. The behavior of a system of isolated chains, with the entire intermolecular potential turned off, was also investigated. In this case, stochastic forces were introduced, and integration was performed as described by van Gunsteren and Berendsen,[31] with a friction constant of 1.33×10^{-3}/fs.

Results and Discussion

Chain Conformation. Table III shows characteristic ratio values (given by $\langle r^2 \rangle / nl^2$, where $\langle r^2 \rangle$ is the mean-square end-to-end distance, n is the number of skeletal bonds, and l is the bond length) computed for PVC melt chains at 450 and 600 K. Results of simulations with and without intermolecular Coulombic interactions and for isolated chains are compared. Values from the rotational isomeric state (RIS) model of Mark[32] are also shown. The simulation values for isolated chains agree quite well with the RIS values. Melt values agree reasonably well with RIS values, with the chains somewhat extended relative to the unperturbed RIS chains. Previous molecular mechanics studies of atactic PVC glasses[12,13] yielded conformations which were compressed, with their mean-square radii of gyration considerably smaller than that for the unperturbed RIS chains. The good agreement with RIS values obtained in the present study may indicate deficiencies in the molecular mechanics methods of generating glass structures or shortcomings in the force-field parameters.

The chains in the melt are somewhat extended relative to isolated chains and chains in the melt without intermolecular Coulombic interactions as indicated in Table III. This effect is more pronounced at the lower temperature. Small-angle neutron scattering studies of glassy PVC[33] indicate that chains are extended in the glass (room temperature) relative to chains in a Θ solvent, with respective characteristic ratio values of 12.64 and 9.68. Characteristic ratio values from the simulations are systematically lower than the experimental values due to the lower molecular weight and higher temperature of the simulations.

Table III also shows the fraction of trans bonds (skeletal bonds with torsional angle between −60° and +60°) as a function of temperature and potential. The fraction of trans bonds varies with temperature and potential in a manner consistent with the characteristic ratio results, with more extended chains having a higher fraction of trans bonds. Agreement between values for the isolated chains and RIS model is good, especially at the higher temperature. The difference at the lower temperature indicates a somewhat stronger temperature dependence of the RIS model.

The distribution of torsional angles in the melt and for isolated chains is shown in Figure 4. Distributions for

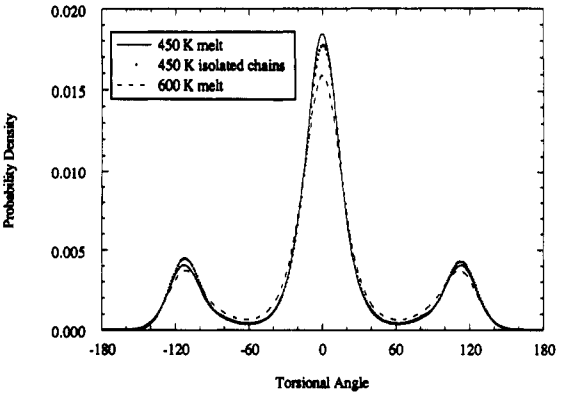

Figure 4. Distribution of torsional angles from simulated melts at 450 and 600 K and isolated chains at 450 K.

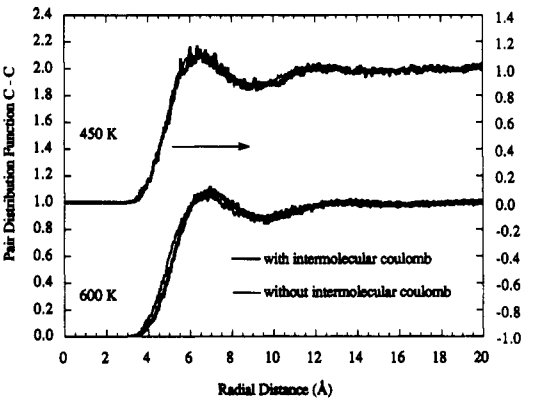

Figure 5. Pair distribution function for C–C. Values at 450 and 600 K computed with the full intermolecular potential and without intermolecular Coulombic interactions are shown.

chains without intermolecular Coulombic interactions lie intermediate to these values. Here, the sign of the torsional angle is uniquely denoted by a right-handed rotation relative to the trans state (trans being 0) independent of the stereochemical nature of the asymmetric center to which the skeletal bond is attached. (Torsional distributions showing populations of the g and ḡ states as defined by Flory and Fujiwara,[34] which yield additional information on the distribution of torsions among non-trans conformational states, will be presented in a future paper considering higher molecular weight PVC.) The distributions of torsional angles are less temperature dependent than those found for polyethylene. This is due to the relatively complex conformational energy surface resulting from the chirality of PVC chains, where a gauche to trans transition does not necessarily lead to lower energy, as it does in polyethylene.

Pair Distribution Functions. Pair distribution functions for C–C, Cl–Cl, Cl–H (methine) and Cl–H (methylene), showing intermolecular correlations only, are shown in Figures 5–8, respectively. Values at 450 and 600 K with and without intermolecular Coulombic interactions are shown. A nearest-neighbor chain separation of approximately 6.5 Å is indicated in the C–C function at 450 K. Eliminating the Coulombic interactions shifts the peak approximately 0.5 Å toward smaller separation. A sharp peak in the Cl–Cl function is seen around 3.5 Å, with the peak being noticeably sharper in the case without Coulombic interactions. The structure seen in the Cl–H (methine) and Cl–H (methylene) pair distribution functions is apparently determined primarily by the topology of the chain segments and the LJ potential as no significant change occurs upon elimination of charges. A slight increase in the magnitude of the first Cl–H (methylene) peak with elimination of the Coulombic interactions can be seen. It is should be noted that in all cases the pair

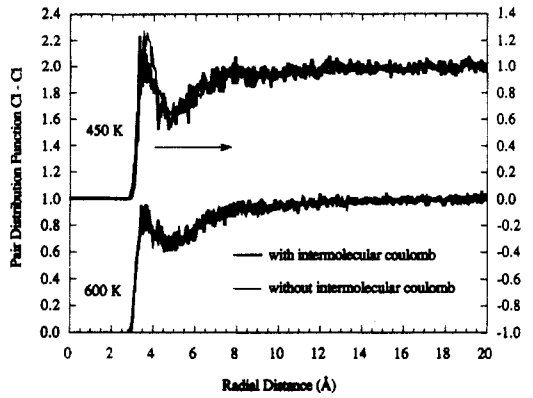

Figure 6. Pair distribution function for Cl–Cl. Values at 450 and 600 K computed with the full intermolecular potential and without intermolecular Coulombic interactions are shown.

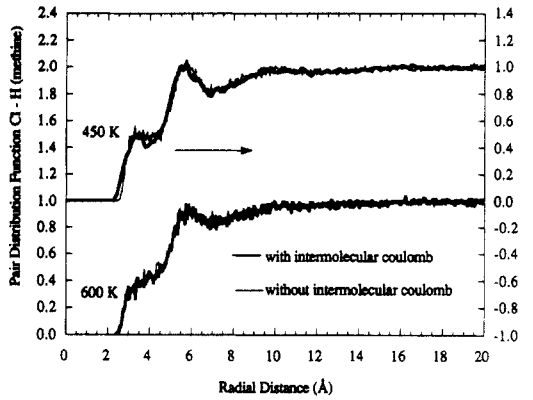

Figure 7. Pair distribution function for Cl–H (methine). Values at 450 and 600 K computed with the full intermolecular potential and without intermolecular Coulombic interactions are shown.

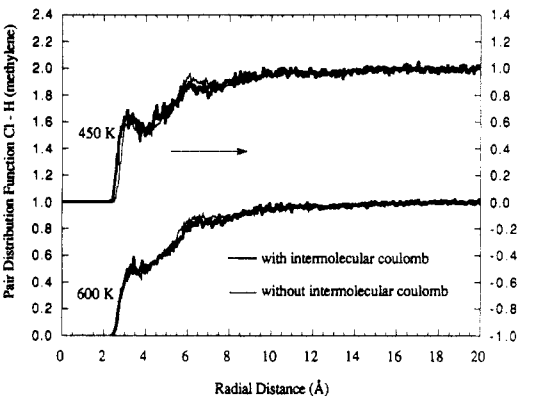

Figure 8. Pair distribution function for Cl–H (methylene). Values at 450 and 600 K computed with the full intermolecular potential and without intermolecular Coulombic interactions are shown.

distribution functions show more pronounced structure with decreasing temperature.

X-ray Structure Factor and Scattering Intensities. X-ray structure factors and scattering intensities can be calculated readily from the pair distribution functions.[35] Figure 9 shows calculated X-ray structure factor profile $S(q)$ for PVC melts at 450 and 600 K for values of the scattering vector $q = 4\pi \sin(\theta/\lambda)$ from 0.5 to 4.0 Å^{-1}, where 2θ is the scattering angle and λ is the wavelength of the X-rays. Qualitative agreement with the experimental profile[36] for atactic PVC glass at 300 K is found for all peaks. Peaks associated with values of $q < 2.5$ Å^{-1}, which are primarily intermolecular in origin, are somewhat shifted relative to experimental positions, most likely due to density differences and finite size effects. The experimental peak for PVC glass at about 1.7 Å^{-1} is significantly stronger ($S(q) = 2.4$) than calculated for the melt at 450 K ($S(q) = 1.2$). Calculated curves show the peak magnitude increasing with decreasing temperature. Intramolecular peak positions ($q > 2.5$ Å^{-1}) agree very well with experiment.

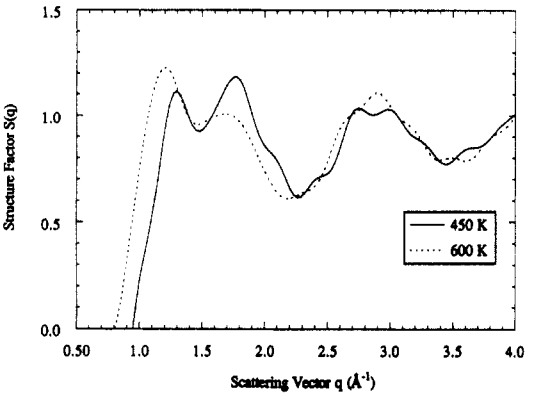

Figure 9. Calculated X-ray structure factor profiles for PVC melts at 450 and 600 K.

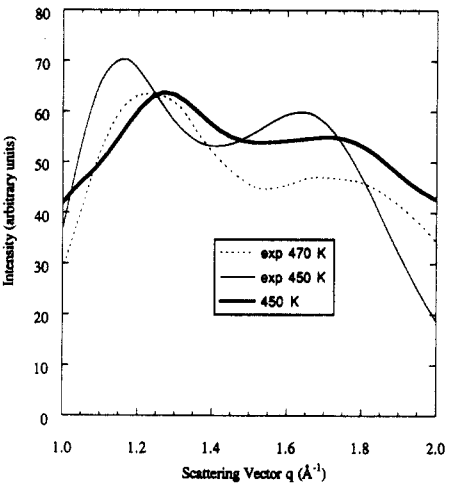

Figure 10. Calculated and experimental X-ray scattering intensities[37] for PVC melts.

Figure 10 shows calculated and experimental[37] X-ray scattering intensities for PVC melts in the region of the internal and external "amorphous" maxima. The two experimental curves correspond to different scan rates (2°/min at 470 K; 1/2°/min at 450 K). Reasonable agreement between the calculated curve for 450 K and experiment is seen. Peak positions agree fairly well, with a slight shift toward larger q values for the calculated curve. Relative peak intensities also agree fairly well with experiment. Discrepancies could be due in part to uncertainties in density. Short-chain effects and finite size effects due to periodic boundary conditions could also contribute.

Intermolecular Orientational Correlation Function. Figure 11 is a plot of the weighted intermolecular orientational correlation function $S_4(R)*G_4(R)$ for four backbone atom segments as a function of distance R between segment centers, where

$$S_4(R) = \frac{1}{2}(3\langle\cos^2\theta\rangle - 1) \qquad (7)$$

and $G_4(R)$ is the pair distribution function for segment centers.[2] The brackets indicate an ensemble average over all segment pairs separated by a distance R. Segment vectors and the intersegmental angle θ are illustrated in Figure 11. Segment vectors connect the centers of the terminal bonds of the segments. Intersegmental distances are measured from the centers of the segment vectors. A value of 1.0 indicates parallel alignment of chain segments, while a value of −0.5 indicates perpendicular alignment.

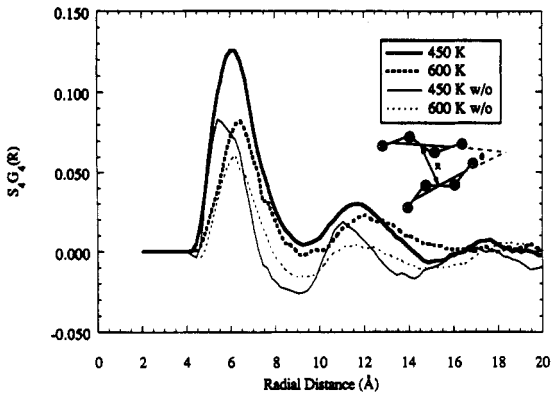

Figure 11. Weighted intermolecular orientational correlation function for PVC melts. Values are for four bond segments at 450 and 600 K, weighted by the pair distribution function for segment centers. Results utilizing the full intermolecular potential and results without intermolecular Coulombic interactions (w/o) are compared.

Results are shown for melts with and without intermolecular Coulombic interactions. Parallel alignment is indicated at distances corresponding to the nearest-neighbor separation, with weaker parallel orientation at the next nearest-neighbor distance. At 450 K emergence of orientational correlation at the third nearest-neighbor distance can be seen. The degree of orientational correlation increases significantly with decreasing temperature. This orientational correlation is strongly influenced by Coulombic interactions, with the degree of parallel order greatly reduced when the Coulombic interactions are excluded from the MD simulations. This also results in a shift in the peak locations by approximately 0.5 Å toward smaller separations. Orientational correlations in PVC melts at 450 K without Coulombic interactions resemble that reported for polypropylene glass from a molecular mechanics simulation.[38]

Orientational Clusters. The intermolecular orientational correlation function indicates a significant degree of parallel-chain alignment in PVC melts. It is not possible to determine from the orientational correlation function whether the parallel segment pairs are distributed homogeneously throughout the bulk or occur in a more localized fashion, perhaps forming small clusters of nearly parallel-chain segments. In order to investigate the distribution of parallel segment pairs, subsets of these pairs were examined graphically. A subset is defined to consist of nearly parallel segment pairs ($S_4(R) > 0.8$) running parallel to an arbitrary direction labeled the z-axis (direction cosine > 0.9 for one of the pairs), and lying within nearest-neighbor separation ($R < 8$ Å) of each other. A typical subset of parallel segments for a system at 450 K is shown schematically in Figure 12. The tendency of nearly parallel segment pairs to occur in small clusters as seen in Figure 12 is typical of the PVC melts at 450 K. A detailed atomistic analysis of this apparent molecular order will be included in a forthcoming paper which considers MD simulations of a higher molecular weight PVC system.

Conclusions

MD simulations of atactic PVC melts were conducted utilizing an ab initio quantum chemistry based atomistic force field. Polar interactions were included by means of partial charges and a distance-dependent dielectric constant to represent Coulombic interactions and dielectric screening effects. All atoms were considered explicitly except for the terminal methyl groups, which were treated as single united atom force centers. Simulation results indicate that chains are extended in the melt relative to isolated chains and melt chains without intermolecular

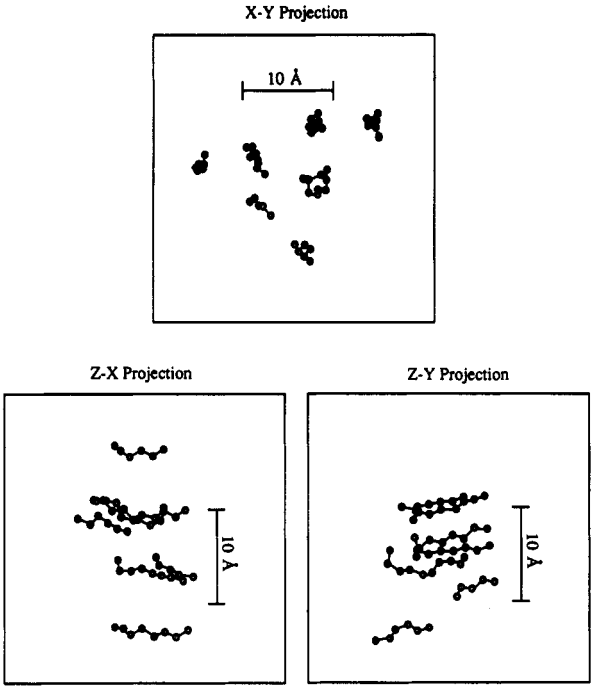

Figure 12. Schematic examples of segment pairs nearly parallel to an arbitrary direction. The arbitrary direction is labeled the z-axis.

Coulombic interactions. Calculated X-ray scattering profiles agree well with experiments. Significant temperature-dependent interchain orientational correlations are seen in PVC melts, with highly parallel segments tending to occur in small localized clusters rather than being homogeneously distributed. These clusters appear to extend at least to second-nearest-neighbor distances, or roughly 12 Å. Finally, it is noted that while polar Coulombic interactions strongly influence intermolecular orientational correlation, the pair distribution functions show only a minor dependence on electrostatic interactions.

Acknowledgment. We gratefully acknowledge Drs. P. Ludovice, R. Winkler, A. D. McLean, and Professor R. H. Boyd for helpful discussions and suggestions regarding simulation and force-field problems.

Appendix

The following is a third-order algorithm for use with the method of Nosé[26] in calculating trajectories in the canonical ensemble. The algorithm is an extension of the van Gunsteren and Berendsen[31] approach to integration of the equations of motion in stochastic dynamics. The motivation behind this integration approach was to provide a method that could easily incorporate stochastic forces and constraints.

We can express the equations of motion given by the extended Hamiltonian of Nosé as

$$m_i\dot{\mathbf{V}}_i = m_i\Theta(t)\,\mathbf{V}_i(t) + \mathbf{F}_i(\mathbf{x}(t)) \qquad \text{(A.1)}$$

where m_i is the mass, $\mathbf{V}_i(t)$ the velocity, and $\mathbf{F}_i(\mathbf{x}(t))$ the systematic force on particle i. $\mathbf{x}(t)$ is the position vector of all particles in the ensemble. $\Theta(t)$ is given by[34]

$$\Theta(t) = -\dot{s}(t)/s(t) \qquad \text{(A.2)}$$

where $s(t)$ is the coordinate of the additional temperature degree of freedom. We wish to know the $\mathbf{x}_i(t)$, the position vector of particle i to third order in δt for each particle. Expanding $\Theta(t)$ yields

$$\Theta(\delta t) = \Theta(0) + \dot{\Theta}(0)\,\delta t + O(\delta t^2) \qquad \text{(A.3)}$$

Substituting eq 2 into eq 1 and integrating yields

$$\mathbf{V}_i(\delta t) = \mathbf{V}_i(0)\exp(\Theta(0)\,\delta t + \dot{\Theta}(0)\,\delta t^2/2) + \exp(\Theta(0)\,\delta t + \dot{\Theta}(0)\,\delta t^2/2)\frac{1}{m_i}\int_0^{\delta t}\exp(-\Theta(0)t - \dot{\Theta}(0)\,t^2/2)\mathbf{F}_i(\mathbf{x}(t))\,dt \quad (A.4)$$

Now let

$$\mathbf{F}_i(\mathbf{x}(t)) = \mathbf{F}_i(t) = \mathbf{F}_i(0) + \dot{\mathbf{F}}_i(0)\,t \quad (A.5)$$

Substituting this expression into eq 3 and integrating yields

$$\mathbf{x}_i(\delta t) = \mathbf{x}_i(0) + I_+\mathbf{V}_i(0) + J_+\mathbf{F}_i(0)/m_i + K_+\dot{\mathbf{F}}_i(0)/m_i \quad (A.6)$$

$$\mathbf{x}_i(-\delta t) = \mathbf{x}_i(0) + I_-\mathbf{V}_i(0) + J_-\mathbf{F}_i(0)/m_i + K_-\dot{\mathbf{F}}_i(0)/m_i \quad (A.7)$$

where

$$I_+ = \int_0^{\delta t}\exp(\Theta(0)t + \dot{\Theta}(0)\,t^2/2)\,dt \quad (A.8)$$

$$J_+ = \int_0^{\delta t}\exp(\Theta(0)\,t + \dot{\Theta}(0)\,t^2/2)\int_0^{\tau}\exp(-\Theta(0)\,\tau - \dot{\Theta}(0)\,\tau^2/2)\,d\tau\,dt \quad (A.9)$$

$$K_+ = \int_0^{\delta t}\exp(\Theta(0)\,t + \dot{\Theta}(0)\,t^2/2)\int_0^{t}\exp(-\Theta(0)\,\tau - \dot{\Theta}(0)\,\tau^2/2)\tau\,d\tau\,dt \quad (A.10)$$

The integrals I_-, J_-, and K_- are obtained by changing the upper limit of integration in the above expressions from δt to $-\delta t$. Solving for $\mathbf{x}_i(\delta t)$ by eliminating $\mathbf{V}_i(0)$ yields

$$\mathbf{x}_i(\delta t) = \mathbf{x}_i(0) + \frac{I_+}{I_-}(\mathbf{x}_i(-\delta t) - \mathbf{x}_i(0)) + \left(J_+ - J_-\left(\frac{I_+}{I_-}\right)\right)\mathbf{F}_i(0)/m_i + \left(K_+ - K_-\left(\frac{I_+}{I_-}\right)\right)\dot{\mathbf{F}}_i(0)/m_i \quad (A.11)$$

Solving for the velocity yields

$$\mathbf{V}_i(0) = I_+(\mathbf{x}_i(-\delta t) - \mathbf{x}_i(0)) + I_-(\mathbf{x}_i(\delta t) - \mathbf{x}_i(0)) + -(I_-J_+ + I_+J_-)\mathbf{F}_i(0)/m_i - (I_-K_+ + {}_{I+}K_-)\dot{\mathbf{F}}_i(0)/m_i \quad (A.12)$$

Constraints are applied in a manner analogous to that described by van Gunsteren and Berendsen.[31] The shaken velocities are obtained from the relationship

$$\mathbf{x}_i' = \mathbf{x}_i + \mathbf{V}_i\mathbf{I}_+ \quad (A.13)$$

We must now consider integration of $\Theta(t)$. Expanding $\Theta(t)$ (as given by eq A.2) as in eq A.3 yields

$$\Theta(0) = -\frac{\dot{s}(0)}{s(0)} \quad (A.14)$$

$$\dot{\Theta}(0) = -\frac{(\ddot{s}(0)\,s(0) - \dot{s}(0)^2)}{s(0)^2} \quad (A.15)$$

where $\ddot{s}(t)$ is given by[26]

$$\ddot{s}(t) = \frac{(T_k(t) - T_f)gk_Bs(t)}{Q} + \frac{\dot{s}(t)^2}{s(t)} \quad (A.16)$$

Here $T_k(t)$ is the kinetic temperature, T_f is the constant temperature of the trajectory, g is the number of degrees of freedom in the system, k_B is Boltzmann's constant, and Q is the mass of the temperature degree of freedom. As determination of $\ddot{s}(0)$ requires knowledge of $\mathbf{V}_i(0)$, the present algorithm cannot be used to integrate $\Theta(t)$. Instead, a fifth-order predictor–corrector algorithm is used, and the predicted values of $\Theta(0)$ and $\dot{\Theta}(0)$ are used in eqs A.8–A.10. Any deviations in the trajectory introduced by this approximation can be minimized by using a reasonably large value of Q. We found a value of 5×10^{-44} J s^2 gave good behavior.

References and Notes

(1) Rigby, D.; Roe, R. J. *J. Chem. Phys.* **1987**, *87*, 7285.
(2) Rigby, D.; Roe, R. J. *J. Chem. Phys.* **1988**, *89*, 5280.
(3) Mansfield, K. F.; Theodorou, D. N. *Macromolecules* **1991**, *24*, 6283.
(4) Rigby, D.; Roe, R. J. In *Computer Simulation of Polymers*; Roe, R. J., Ed.; Prentice-Hall: Englewood Cliffs, NJ, 1991; pp 79–93.
(5) Takeuchi, H.; Roe, R. J. *J. Chem. Phys.* **1991**, *94*, 7446.
(6) Takeuchi, H.; Roe, R. J. *J. Chem. Phys.* **1991**, *94*, 7446.
(7) Sylvester, M. F.; Yip, S.; Argon, A. S. In *Computer Simulation of Polymers*; Roe, R. J., Ed.; Prentice-Hall: Englewood Cliffs, NJ, 1991; p 105–121.
(8) Pant, P. V. K.; Boyd, R. H. *Macromolecules* **1992**, *25*, 494.
(9) Smith, G. D.; Boyd, R. H. *Macromolecules* **1992**, *25*, 1326.
(10) Candau, S. J.; Dormoy, Y.; Hirsh, E.; Mutin, P. H.; Guenet, J. H. *Reversible Polymeric Gels and Related Systems*; Russo, P. S., Ed.; 1981; Vol. 33, p 350.
(11) Juijin, J. A.; Gisolf, J. H.; de Jong, W. A. *Kolloid Z. Z. Polym.* **1973**, *251*, 456.
(12) Ludovice, P. J.; Suter, U. W. In *Computational Modeling of Polymers*; Bicerano, J., Ed.; Marcel Dekker: New York, 1992; pp 401–435.
(13) Lee, K. J.; Mattice, W. L. *Comput. Polym. Sci.* **1992**, *2*, 55.
(14) Jaffe, R. L.; Ludovice, P. J.; Smith, G. D.; Yoon, D. Y. Derivation of a Force Field for Polymeric and Oligomeric Vinyl Chloride Based on Ab Initio Quantum Chemistry. In preparation.
(15) Jaffe, R. L.; Smith, G. D.; Yoon, D. Y. The Use of Second Virial Coefficients in the Parameterization of Intermolecular Potential Energy Functions. In preparation.
(16) Williams, D. E.; Cox, S. R. *Acta Crystallogr., Sect. B* **1984**, *40*, 404.
(17) Williams, D. E.; Hsu, L. Y. *Acta Crystallogr., Sect. A* **1985**, *41*, 296.
(18) Mayo, S. L.; Olafson, B. D.; Goddard, W. A., III *J. Phys. Chem.* **1990**, *94*, 8897.
(19) Dymond, J. H.; Smith, E. B. *The Virial Coefficients of Gases*; Clarendon: Oxford, 1969.
(20) Block, H.; Walker, S. M. *Chem. Phys. Lett.* **1973**, *19*, 363.
(21) Rutledge, G. C.; Suter, U. W. *Macromolecules* **1991**, *24*, 1921.
(22) Andrea, T. A.; Swope, W. C.; Andersen, H. C. *J. Chem. Phys.* **1983**, *79*, 4576.
(23) Adams, D. J.; Adams, E. M.; Hills, G. J. *Mol. Phys.* **1979**, *38*, 387.
(24) Flory, P. J.; Mark, J. E.; Abe, A. *J. Am. Chem. Soc.* **1966**, *88*, 639.
(25) Carman, C. J. *Macromolecules* **1973**, *6*, 725.
(26) Nosé, S. *J. Chem. Phys.* **1984**, *81*, 512.
(27) Ishinabe, T.; Ishikawa, K. *Jpn. J. Appl. Phys.* **1968**, *7*, 472.
(28) Ryckaert, J. P.; Ciccotti, G.; Berendsen, H. J. C. *J. Comput. Phys.* **1977**, *23*, 327.
(29) Ryckaert, J. P. *Mol. Phys.* **1985**, *3*, 549.
(30) Brandrup, J.; Immergut, E. H. *Polymer Handbook*; John Wiley and Sons: New York, 1987; p 553.
(31) van Gunsteren, W. F.; Berendsen, H. J. C. *Mol. Phys.* **1982**, *45*, 637.
(32) Mark, J. E. *J. Chem. Phys.* **1972**, *69*, 451.
(33) Herchenroeder, P.; Dettenmaier, M.; Fischer, E. W.; Stamm, M.; Haas, J.; Reimann, H.; Tieke,; Wegner, G.; Zichne, E. L. *Chem. Abstr.* **1978**, *89*, 198133.
(34) Flory, P. J.; Fujiwara, Y. *Macromolecules* **1969**, *2*, 315.
(35) Wagner, C. N. J. *J. Non-Cryst. Solids* **1978**, *31*, 1.
(36) Ludovice, P. J.; Suter, U. W.; Maeda, T.; Egami, T.; Papaspyrides, C. D. Unpublished data.
(37) Guerrero, S. J.; Meader, D.; Keller, A. *J. Macromol. Sci., Phys.* **1981**, *B20*, 185.
(38) Theodorou, D. N.; Suter, U. W. *Macromolecules* **1985**, *18*, 1467.